

Flow patterns and pressure gradient correlation for oil–water core–annular flow in horizontal pipes

Haili Hu^{1,2} (✉), Jiaqiang Jing^{1,3} (✉), Jiatong Tan¹, Guan Heng Yeoh²

1. State Key Laboratory of Oil and Gas Reservoir Geology and Exploitation, Southwest Petroleum University, Chengdu 610500, China

2. School of Mechanical and Manufacturing Engineering, University of New South Wales, Sydney, NSW 2052, Australia

3. Oil & Gas Fire Protection Key Laboratory of Sichuan Province, Chengdu 611731, China

Abstract

The water-lubricated transportation of heavy oil seems to be an attractive method for crude oil production with significant savings in pumping power. With oil surrounded by water along the pipe, oil–water core–annular flow forms. In this paper, the characteristics of oil–water core–annular flow in a horizontal acrylic pipe were investigated. Plexiglas pipes (internal diameter = 14 mm and length = 7.5 m) and two types of white oil (viscosity = 0.237 and 0.456 Pa·s) were used. Flow patterns were observed with a high-speed camera and rules of flow pattern transition were discussed. A pressure loss model was modified by changing the friction coefficient formula with empirical value added. Totally 224 groups of experimental data were used to evaluate pressure loss theoretical models. It was found the modified model has been improved significantly in terms of precision compared to the original one. With 87.4% of the data fallen within the deviation of $\pm 15\%$, the new model performed best among the five models.

Keywords

oil–water flow
core–annular flow (CAF)
flow pattern transition
pressure gradient
empirical correlations

Article History

Received: 10 May 2019

Revised: 3 July 2019

Accepted: 3 July 2019

Research Article

© Tsinghua University Press 2019

1 Introduction

With the increase of world energy consumption and the decline of conventional oil storage in recent years, heavy oil becomes increasingly important (Lanier, 1998). Heavy oil represents at least half of the recoverable oil resources worldwide (Martínez-Palou et al., 2011). However, the production, transportation, and refining of heavy oil are greatly limited by its high viscosity (commonly more than 200 cp at reservoir conditions). High viscosity during transport means more pump energy consumption and thus higher exploitation costing. Conventional methods including heating, dilution, and emulsification have been tested to enhance the economy of transport (Sanieri et al., 2004), but these methods are either expensive or environmentally unfriendly. Some of them even need subsequent processing such as demulsification (Martínez-Palou et al., 2011). Water-lubricated transport of heavy oil seems to be a promising technique to solve the problem (Bannwart, 2001; Prada and Bannwart, 2001; Ghosh et al., 2009; Rodriguez et al., 2009).

With oil flowing in the center and water flowing as an annulus, oil–water core–annular flow (CAF) forms. The drag force drops dramatically. As reported, a maximum of 90% reduction in pressure loss has been achieved within annular flow (Bensakhria et al., 2004).

Due to the low pressure loss and energetic advantage, CAF has been attracting intensive research attention. The first discussion about water lubrication of oil can be dated back to 1904 (Isaac and Speed, 1904), but experimental and theoretical research on CAF was not started until the 1960s. In the pioneering experimental study of Charles et al. (1961), CAF was observed in addition to oil slugs in water, oil bubbles in water, and oil drops in water. Thanks to the series of studies carried by them, the advantages of the core-flow technology have been fully appreciated. CAF is getting more attention in the experimental study of scholars. Typical CAF patterns including perfect CAF, wavy CAF, disturbed wave CAF, and perturbed wavy CAF were noted (Bai et al., 1992; Arney et al., 1993; Bannwart et al., 2004; Sotgia et al., 2008).

✉ H. Hu, haimoly@163.com; J. Jing, jjq@swpu.edu.cn

Nomenclature

dP/dx	pressure gradient (Pa/m)
D	diameter (m)
Q	volumetric flow rate (m ³ /s)
u	velocity (m/s)
Re	Reynolds number
Fr	Froude number
Eo'	Eötvös number
H	holdup
k	constant
C	constant
APE	average percent error
AAPE	average absolute percent error
SD	standard deviation
X^2	Martinnelli coefficient
ε	pipe wall roughness (m)

Greek symbols

Δ delta

μ	viscosity (Pa·s)
ρ	density (kg/m ³)
λ	friction coefficient
ϕ	input volume fraction
ξ	pressure loss ratio

Subscripts

w	water phase
o	oil phase
m	mixture
sw	superficial water
so	superficial oil
sm	superficial mixture
a	annulus phase
c	core phase
as	annulus superficial
cs	core superficial

However, in the oil–water flow system, CAF does not always appear. It exists under certain circumstances, affected by the flow rate, density, viscosity ratio, and interfacial tension between fluids (Joseph et al., 1984; Georgiou et al., 1992; Bannwart, 2001; Rodriguez and Bannwart, 2008; Tripathi et al., 2015). For a particular diameter of the pipe, it is common to see flow pattern transition within a limited range of fluid velocities and water fraction (Tan et al., 2018). As an unstable flow pattern, the transitions from other flow patterns to CAF or from CAF to other flow patterns are more likely to occur, which should be studied to reduce. Several researchers have conducted experimental studies on oil–water flow in horizontal pipes with CAF observed (Ooms et al., 1983; Oliemans et al., 1987; Arney et al., 1993; Joseph et al., 1999; Bannwart et al., 2004; Grassi et al., 2008; Sotgia et al., 2008; Strazza et al., 2011). Flow pattern transition and criteria for the existence of CAF were discussed (Joseph et al., 1984; Brauner and Moalem Maron, 1992; Bannwart, 2001; Bannwart et al., 2004; Grassi et al., 2008). These previous studies were mostly limited to pipes with internal diameter sizes above 20 mm, or low viscosity oils (less than 100 cp) or high viscosity oils (more than 1000 cp). The investigation on the medium viscosity oil in smaller pipes is still lacking.

Pressure loss prediction of annular flow is essential for accurate design and optimization of multi-phase flow systems (Singh and Lo, 2010; Li et al., 2013). Since Russel and Charles (1959) proposed a simple theoretical model to calculate the perfect annular flow, several theoretical

or semi-theoretical/semi-empirical formulas have been presented to compute the pressure loss of CAF (Ooms et al., 1983; Oliemans et al., 1987; Arney et al., 1993; Bannwart, 1999; McKibben et al., 2000). These models can also be divided into two categories: the empirical/phenomenological models and the mechanistic models. The former models treat the oil–water flow as a mixed fluid, using empirical correlations, while the latter models treat the immiscible fluids separately by using more complicated formulas (Shi, 2015). Most models do not take into account the effects of oil fouling and eccentricity, which have been observed in the literature (Arney et al., 1993; Grassi et al., 2008). These models tend to underestimate the pressure loss by ignoring these phenomena (Shi, 2015). Therefore, new models are needed, especially empirical models, for they are easier to use compared to mechanism models.

In this work, efforts have been made to investigate the flow patterns of two types of white oil in horizontal pipes with an internal diameter of 14 mm. Rules of flow pattern transition were discussed. To improve the prediction accuracy of pressure loss, a simple empirical model was modified, adding the impact of oil fouling and eccentricity on pressure loss. An empirical correlation for the friction factor was proposed combining oil viscosity, Reynolds number, and pipe wall roughness together. 224 groups of data were used in the comparison between pressure loss models and experimental results. Results show that the new model performed the best, and 87.4% of the data fell within the deviation of $\pm 15\%$.

2 Experiment and method

2.1 Working fluids

In the present study, tap water and industry white oil were used. White oil, also called mineral oil, is a mixture of liquid hydrocarbons obtained from crude oil by different methods of distillation and refining. Due to the different distillation ranges, hydrocarbons with various molecular weights are separated and condensed into different products (Marinescu et al., 2012), making physical properties of white oils different. In this study, W-200 and W-400 white oils from Shenzhen Huameite Lubrication Technology Company were used. The two types of oils were featured by the density of 869.6 and 896.2 kg/m³, the viscosity of 0.237 and 0.456 Pa·s, and the interfacial tension between oil and water of 45.83 and 51.49 mN/m (all at 25 °C), respectively. The density and viscosity of tap water at 25 °C are 999 kg/m³ and 0.001 Pa·s, respectively. Physical properties of the test fluids are reported in Table 1.

2.2 Experimental setup

The schematic of the experimental facility is shown in Fig. 1. The oil and water were stored in an oil tank and a water tank, respectively. The oil flow was pumped by a gear pump (Shengyuan, KCB-55), then metered by a gear flowmeter (Meikong, MIK-A, flow rate range 0–3.0 m³/h

and accuracy $\pm 0.15\%$). The water flow was pumped by a vortex pump (Yangzijiang, 32W-120), then metered by a turbine flowmeter (Meikong, MIK-LWGY-DN10, flow rate range 0–1.5 m³/h and accuracy $\pm 1\%$). The oil and water met at the T-junction, then entered the main part of the facility, the acrylic pipeline with a length of 7.5 m and an internal diameter of 14 mm.

The pipeline was divided into a developing section (length = 3 m), a test section (length = 3 m), and an observation section (length = 1.5 m). Since the pipe length of the developing section was 206 times greater than its internal diameter, the flow was deemed to be fully developed. A differential pressure transducer (Rosemount, pressure range 0–62.16 kPa and accuracy $\pm 0.065\%$) was attached to both ends of the test section pipe to measure the pressure drop.

The flow patterns were recorded by a high-speed camera (Revealer 2F04C) located in the observation section. The recording speed was 379 f/s. Temperature transducers (Meikong, YCHSM-200, temperature range 0–100 °C and accuracy $\pm 0.05\%$) were adopted to measure the temperature of oil and water. Signals including flow rate, pressure drop, and temperature were collected by a paperless recorder (Huiteng, 8 channels). To make the data more reliable, experimental data and photographs were recorded after the test parameters stabilized for 10 min. All experiments were carried out at 25 °C.

After the oil and water departed from the test section and entered the separation tank, they were pumped and transported back to the oil tank and water tank, respectively. Then the residual oil and water in the pipe were cleaned by water and pressurized air.

Table 1 Properties of the test fluids

Property	White oil		Water
	W-200	W-400	
Density (kg/m ³ , 25 °C)	869.6	896.2	999
Viscosity (Pa·s, 25 °C)	0.237	0.456	0.001
The interfacial tension between oil and water (mN/m)	45.83	51.49	—

2.3 Pressure gradient modeling

2.3.1 PCAF model

In 1959, Russel and Charles put forward the perfect CAF

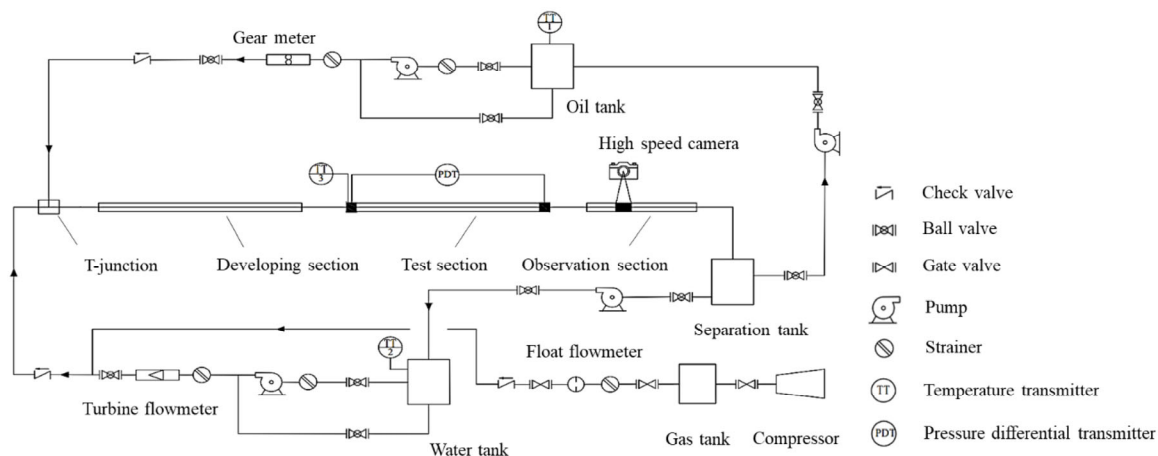


Fig. 1 Schematic of the experimental facility.

(PCAF) model (Russell and Charles, 1959). The model hypothesizes that both oil core and water annulus are laminar flows, ignoring the influence of eccentricity and interface waves. The frictional pressure gradient can be expressed as

$$-\frac{dP}{dx} = \frac{128\mu_w Q_m}{\pi D^4 \left[1 - \left(1 - \frac{\mu_w}{\mu_o} \right) H_o^2 \right]} \quad (1)$$

$$Q_m = Q_o + Q_w \quad (2)$$

$$H_o = \frac{1}{1 + (Q_w / Q_o) \left[1 + \sqrt{1 + (\mu_w / \mu_o)(Q_o / Q_w)} \right]} \quad (3)$$

where Q_m is the total flow rate of oil and water; Q_w is the flow rate of water; Q_o is the flow rate of oil; D is the pipe diameter; H_o is the oil holdup; and μ_w and μ_o are the viscosity of water and oil, respectively.

At $\mu_w / \mu_o \ll Q_w / Q_o < 1$, the oil holdup and pressure loss can be approximately expressed as

$$-\frac{dP}{dx} = \frac{128\mu_w Q_m}{\pi D^4 (1 - H_o^2)} \quad (4)$$

$$H_o = \frac{1}{1 + 2Q_w / Q_o} \quad (5)$$

2.3.2 The model of Arney

Arney modified the friction coefficient formula by deducing a counterpart similar to the Reynolds number without considering the effect of interface waves and eccentric (Arney et al., 1993). An empirical correlation for calculating the water holdup is given in this model. The pressure loss is calculated as

$$-\frac{dP}{dx} = \frac{\lambda_{Arney} \rho_m u_{sm}^2}{D} \quad (6)$$

where λ_{Arney} is the friction coefficient; ρ_m is the mixture density; and u_{sm} is the mixture velocity.

When the mixture velocity occurred at the laminar flow and turbulent flow, λ_{Arney} is given as

$$\text{Laminar flow} \quad \lambda_{Arney} = \frac{64}{\mathcal{R}} \quad (7)$$

$$\text{Turbulent flow} \quad \lambda_{Arney} = \frac{0.316}{\mathcal{R}^{0.25}} \quad (8)$$

where \mathcal{R} is defined as

$$\mathcal{R} = \frac{\rho_m u_{sw} D}{\mu_w} \left[1 + \eta^4 \left(\frac{\mu_w}{\mu_o} - 1 \right) \right] \quad (9)$$

$$\eta = \sqrt{1 - H_w} \quad (10)$$

The mixture density ρ_m is expressed as

$$\rho_m = H_w \rho_w + (1 - H_w) \rho_o \quad (11)$$

where ρ_w is the viscosity of water; ρ_o is the viscosity of oil; H_w is the water holdup. The water holdup can be obtained as

$$H_w = \phi_w [1 + 0.35(1 - \phi_w)] \quad (12)$$

where ϕ_w is the input water volume fraction.

2.3.3 The model of Bannwart

Bannwart modified the PCAF model and put forward a new model (Bannwart, 1999). The model considers water annulus as a turbulent flow with the effect of interface waves considered. It is expressed as

$$-\frac{dP}{dx} = \frac{\Delta P_w \phi_w^{-m}}{L} \quad (13)$$

where ΔP_w is the pressure loss generated when single-phase water flows at the mixture velocity u_{sm} ; m is an empirical parameter associated with pipe material ($m = 0.1$ for oleophobic pipes, $m = 0.286$ for oleophilic pipes). ϕ_w is defined as

$$\phi_w = \frac{u_{sw}}{u_{sw} + u_{so}} = \frac{Q_w}{Q_w + Q_o} \quad (14)$$

ΔP_w follows:

$$-\Delta P_w = \frac{\lambda_w \rho_w u_{sm}^2 L}{2D} \quad (15)$$

$$\lambda_w = \frac{0.316}{Re_w^{0.25}} \quad (16)$$

$$Re_w = \frac{u_{sm} \rho_m D}{\mu_w} \quad (17)$$

where λ_w is the water-phase friction coefficient; ρ_w is the density of water; Re_w is the Reynolds number of water.

2.3.4 The model of Brauner

Brauner put forward the pressure loss formula of concentric CAF flow based on the two-fluid model (Brauner, 1991, 1998). The model ignores the effect of entrainment, eccentricity, and waveform interface. The pressure loss ratio between the oil–water CAF and single-phase oil core in horizontal pipes can be expressed as

$$\xi_c = \frac{(dP/dz)}{(dP/dz)_{cs}} = \frac{X^2}{(1 - \tilde{D}_c^2)^2} \quad (18)$$

where X^2 is the Martinelli coefficient defined as $(dP/dz)_a/$

(dP/dz) ; \tilde{D}_c is the diameter ratio defined as $\tilde{D}_c = D_c/D$. When the flow in the water annulus is turbulent, X^2 and \tilde{D}_c can be calculated as

$$X^2 = \frac{0.046 \left(\frac{\mu_w}{\mu_o} \right) Re_{as}^{0.8}}{16 \tilde{J}} \tag{19}$$

$$\tilde{D}_c^2 = \frac{\tilde{J} + C_i / 2 \left[1 - (1 + 4X^2 \tilde{J}^2 / C_i^2)^{0.5} \right]}{C_i + \tilde{J} - X^2 \tilde{J}} \tag{20}$$

where Re_{as} is the Reynolds number of water annulus at superficial velocity; \tilde{J} is u_c/u_a ; and C_i is 1.15/1.2.

3 Results and discussion

3.1 Flow regime observations

Flow patterns observed in two experimental runs which are representative of most observation are shown in Figs. 2 and 3. The water superficial velocity u_{sw} is controlled constant while oil superficial velocity u_{so} is gradually increased.

In Figs. 2 and 3, when the oil superficial velocity is low ($u_{so} \leq 0.1$ m/s), the oil is dispersed in the spherical or spherical-like form in the water, forming bubbly flow (Figs. 2(a) and 3(a)). Along with the increase of oil superficial velocity (W-200 white oil, $u_{so} \leq 0.35$ m/s; W-400 white oil, $u_{so} \leq 0.68$ m/s), the oil drops assemble and exist in the form of short oil plug and long oil plug in the water (Figs. 2(b) and 3(b)), forming plug flow (Fig. 3(c)) and semi-annular flow (Figs. 2(c) and 3(d)). With the oil superficial velocity further rising, the long-plug-shaped oil is connected into the oil core, forming CAF (Figs. 2(d) and 3(e)). The annular flow observed in the experiments is wavy core–annular flow (WCAF). It is believed waves created at the water and oil interface lead to WCAF (Bai et al., 1992; Bannwart, 2001), but the mechanism is still unclear.

When the oil superficial velocity is low (W-200 white oil, $u_{so} = 0.42$ m/s; W-400 white oil, $u_{so} = 0.74$ m/s), CAF is eccentric (Figs. 2(d) and 3(e)). This is mainly because the density difference between oil and water leads to the generation of buoyancy; the inertia force at low oil superficial velocity is small, making the buoyancy force become dominant. The eccentricity degree of oil cores can be determined by the Froude number (Shi and Yeung, 2017). The Froude number is the ratio of the inertial force to the buoyancy force and is defined as follows:

$$Fr = \frac{u_{so}}{\sqrt{gD \frac{\Delta\rho}{\rho_w}}} \tag{21}$$

where u_{so} is the superficial velocity of oil; $\Delta\rho$ is the density

differential; g is the gravitational acceleration; D is the pipe internal diameter; and ρ_w is the water density.

The oil inside the water is inclined to be concentric when the inertial force is dominant and eccentric when the buoyancy force is dominant. When the oil superficial velocity further rises, the proportion of oil phase in the pipes increases, and only a thin layer of water films exists between the oil core and the upper-layer pipe walls (Figs. 2(f) and 3(f)). At this moment, the inertia force is intensified, making the oil core more concentric.

3.2 Flow pattern maps

The flow pattern maps for W-200 and W-400 white oils are shown in Figs. 4 and 5, respectively (Tan et al., 2018). Looking at the figures in detail, bubble flow (Bo), plug flow (PLo), semi-annular flow (Semi-Anw), and annular flow (Anw) are observed in both experiments, while wave stratified flow (SW) only appears in the oil–water flow of W-200 white oil. This is because gravity is dominant in SW flow, while the

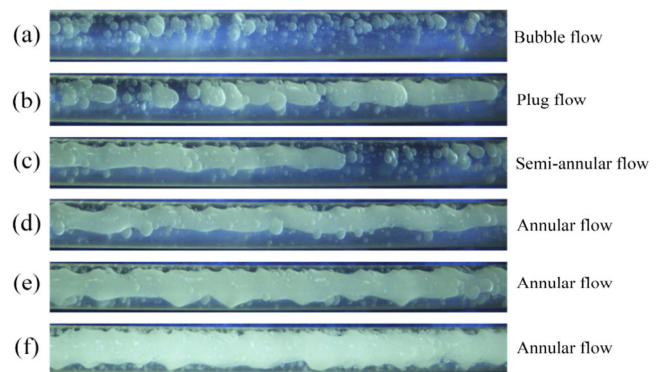


Fig. 2 Flow patterns observed for W-200 white oil with water superficial velocity $u_{sw} = 1.00$ m/s: (a) $u_{so} = 0.13$ m/s, (b) $u_{so} = 0.27$ m/s, (c) $u_{so} = 0.35$ m/s, (d) $u_{so} = 0.42$ m/s, (e) $u_{so} = 0.79$ m/s, (f) $u_{so} = 1.27$ m/s.

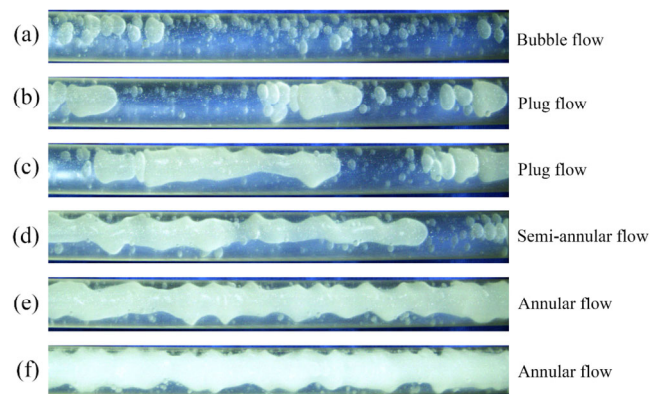


Fig. 3 Flow patterns observed for W-400 white oil with water superficial velocity $u_{sw} = 1.17$ m/s: (a) $u_{so} = 0.13$ m/s, (b) $u_{so} = 0.19$ m/s, (c) $u_{so} = 0.39$ m/s, (d) $u_{so} = 0.52$ m/s, (e) $u_{so} = 0.84$ m/s, (f) $u_{so} = 1.38$ m/s.

interfacial tension is dominant in oil–water flow with higher oil viscosity.

As shown in Fig. 4, flow patterns are more diverse when the oil superficial velocity is low ($u_{so} \leq 0.5$ m/s). For lower oil superficial velocity (i.e., $u_{so} = 0.1$ m/s), transitions occur from SW to Bo, then to Do/w flow, with the increase of water superficial velocity. For higher oil superficial velocity ($u_{so} \geq 1$ m/s), flow patterns narrow to Do/w and Anw flows. A similar phenomenon can be seen in Fig. 5. PLo, Bo, and Semi-Anw flows are observed when the oil superficial velocity is lower than 0.5 m/s, while Anw flow is observed as the oil superficial velocity grows above 0.8 m/s.

Comparing Figs. 4 and 5, the region of Anw flow for W-400 white oil is larger than that for W-200 white oil, which means Anw flow is more likely to appear in the oil–water flow of W-400 white oil. As mentioned above, studies have been carried out on the existence of core flow, which generally indicate three conditions accounting for the formation of CAF (Bannwart, 2001): (1) The core phase must be much thicker than the annulus; (2) water annulus must persist

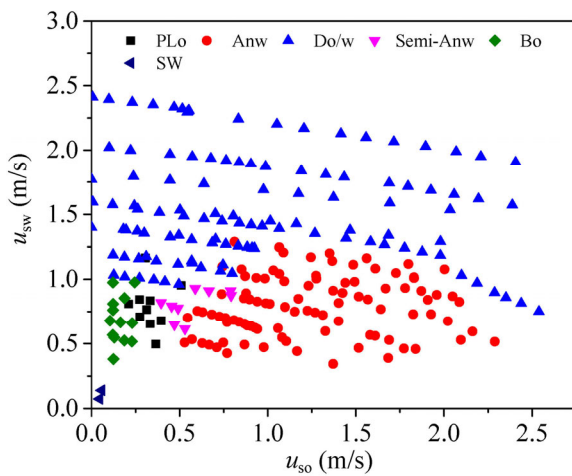


Fig. 4 Flow pattern maps of oil–water flow for W-200 white oil.

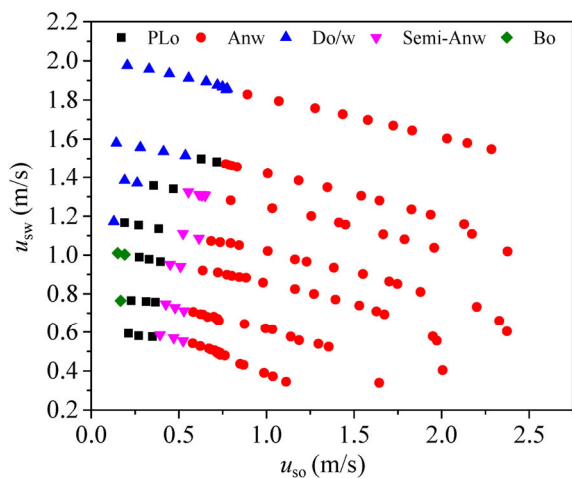


Fig. 5 Flow pattern maps of oil–water flow for W-400 white oil.

and prevent the contact between the oil core and pipe walls; (3) water content must not be too high, otherwise water annulus-induced waves would break down the oil core. Many researchers have tried to quantify the boundaries of CAF. In Bannwart's view, at $Eo' < \frac{4}{\pi\varepsilon}$, stable CAF would exist, and ε is the volume fraction of oil core. Eo' is the Eötvös number, and defined as follows (Brauner and Moalem Maron, 1999):

$$Eo' = \frac{\Delta\rho g D^2}{8\sigma} \quad (22)$$

where σ is the interfacial tension.

As shown in Eq. (22), the existing boundaries of CAF are affected by the density difference between oil and water, pipe diameter, and the interfacial tension between oil and water. For the oil–water flow of W-200 and W-400 oils, the calculated values of Eo' are 0.54 and 0.48, respectively, extending the existing region of CAF for W-400 white oil to a condition where the volume fraction of the core is smaller.

3.3 Pressure gradient modeling

3.3.1 Proposed model

The eccentricity occurs in horizontal CAF flow, due to the density difference between oil and water. When the velocity is low, the oil core tends to float upwards, causing oil adhered to the pipe wall. Besides, when operating conditions change, such as experiencing a sudden shutdown, the oil will also adhere to the wall. The contamination of the pipe wall is often recognized as oil fouling. As CAF flows in the contaminated pipe, the water is in direct contact with the oil film adhered to the wall, instead of the wall itself, which means a change in the roughness of the pipe wall. In addition, the shear between the top side of the oil core and the thin water layer becomes much higher because of the eccentricity of the oil (Shi, 2015). Empirical correlations for the friction factor considering oil fouling and eccentricity should be proposed.

The model of Bannwart is simple and can calculate CAF pressure loss by only using single-phase water pressure loss. However, the model did not take oil fouling and eccentricity into account. The friction coefficient of the model needs to be improved. Many efforts have been devoted to the computation of the friction coefficient in the literature. Moody (1947), Jain (1976), and Schorle et al. (1980) put forward simple explicit equations, while Chen (1979), Zigrang and Sylvester (1982), and Serghides (1984) proposed numerical algorithms. More complicated equations mean more precise predicting results. However, the accuracy and complexity in practice should be balanced. Angeli

and Hewitt (1999) found the roughness of acrylic pipes was highly consistent with the calculated results from the Zigrang and Sylvester equation (Al-Wahaibi, 2012). It can be expressed as

$$\frac{1}{\lambda_m} = 4 \log \left(\frac{\varepsilon/D}{3.7} - \frac{4.518}{Re_m} \log \left(\frac{6.9}{Re_m} + \left(\frac{\varepsilon/D}{3.7} \right)^{1.11} \right) \right) \quad (23)$$

$$Re_m = \frac{u_{sm} \rho_m D}{\mu_m} \quad (24)$$

where λ_m is the mixture friction coefficient; Re_m is the mixture Reynolds number; ε is the pipe wall roughness; and μ_m is the mixture viscosity.

Due to the effects of surface wettability, limitations of constant m , and oil film adhering to the pipe wall, we re-defined the friction coefficient:

$$\frac{1}{\lambda_w} = 4 \log \left(\frac{k\varepsilon/D}{3.7} - \frac{4.518}{Re_w} \log \left(\frac{6.9}{Re_w} + \left(\frac{k\varepsilon/D}{3.7} \right)^{1.11} \right) \right) \quad (25)$$

where λ_w is the single-phase water friction coefficient; Re_w is the single-phase water Reynolds number; k is an empirical coefficient considering oil fouling and eccentricity; k is related to the oil viscosity ($k = 0.23\mu_o + 125$) and can be determined from the data in Table 2.

3.3.2 Model evaluation

To evaluate the prediction precision of these models mentioned above, average percent error (APE), average absolute percent error (AAPE), and standard deviation (SD) are used to evaluate the computational precision (Al-Wahaibi et al., 2014). APE is used to quantify the deviation degree of the predicted value from the experimental value. A positive APE means the predicted value is larger, and vice versa. AAPE is to evaluate the prediction capability of the correlation. The dispersion degree of predicted data relative to experimental data is evaluated by SD. The equations are listed as follows:

$$APE = \left[\frac{1}{n} \sum_{k=1}^n \frac{(dP/dx)_{pred} - (dP/dx)_{exp}}{(dP/dx)_{exp}} \right] \times 100 \quad (26)$$

$$AAPE = \left[\frac{1}{n} \sum_{k=1}^n \left| \frac{(dP/dx)_{pred} - (dP/dx)_{exp}}{(dP/dx)_{exp}} \right| \right] \times 100 \quad (27)$$

$$SD = \sqrt{\frac{1}{n-1} \sum_{k=1}^n \left(\frac{(dP/dx)_{exp} - (dP/dx)_{pred}}{(dP/dx)_{exp}} \right)^2} \times 100 \quad (28)$$

where $(dP/dx)_{pred}$ is the predicted pressure drop; $(dP/dx)_{exp}$ is the experimental pressure drop.

3.3.3 Comparison with experimental results

Totally 110 groups of CAF pressure loss data from literature (Oliemans et al., 1985; Grassi et al., 2008; Sotgia et al., 2008; Al-Wahaibi et al., 2014) and 114 groups of data in our study were used to evaluate the prediction precision of pressure loss models. The experimental data involved the oil viscosity from 12 to 3000 mPa·s, pipe diameter from 14.5 to 50.0 mm, the oil superficial velocity from 0.20 to 2.37 m/s, and the water superficial velocity from 0.03 to 1.68 m/s. The roughness of Plexiglas pipes was 1×10^{-5} m. The experimental data of oil–water CAF in horizontal pipes are shown in Table 2. Comparison of the accuracies of pressure gradient prediction of five models against experimental data from the different sources is shown in Fig. 6. To better evaluate the performance of the models, the average APE, AAPE, SD for all experimental data are computed, and the results are shown in Table 3.

As shown in Fig. 6 and Table 3, the prediction accuracy of the PCAF model (the average AAPE = 93.3%) is the lowest. It is because the model hypothesizes both oil core and water annulus are laminar flows while the water annulus in the experiment is mainly turbulent flow. Among the five models, the average APE, AAPE, SD values of the modified Bannwart model for the 224 groups of data are the lowest, which means the model has the highest prediction accuracy.

The prediction accuracy of the modified Bannwart model had improved significantly by adopting the new friction coefficient Eq. (25), compared to the original one. It can be seen from Fig. 6 that the APE, AAPE, and SD values had dropped dramatically after the modification for each set of data, especially for data from Al-Wahaibi and

Table 2 Database for oil–water core–annular flow in horizontal pipes

Data source	μ_o (mPa·s)	ρ_o (kg/m ³)	D (mm)	Oil type	Pipe material	The interfacial tension between oil and water (mN/m)	ϕ_{wmin} (%)	ϕ_{wmax} (%)
W-200	237	870	14.5	Mineral oil	Acrylic	45.8	18.8	71.0
W-400	456	896	14.5	Mineral oil	Acrylic	51.5	16.8	64.5
Grassi et al. (2008)	799	886	21.0	Mineral oil	PVC	50.0	19.1	81.5
Sotgia et al. (2008)	919	889	26.0	Mineral oil	Plexiglass	20.0	38.4	78.5
Al-Wahaibi et al. (2014)	12	870	19.0	Mineral oil	Acrylic	20.1	52.2	76.6
Oliemans et al. (1985)	3000	978	50.0	Crude oil	Perpex	40	5.0	20.0

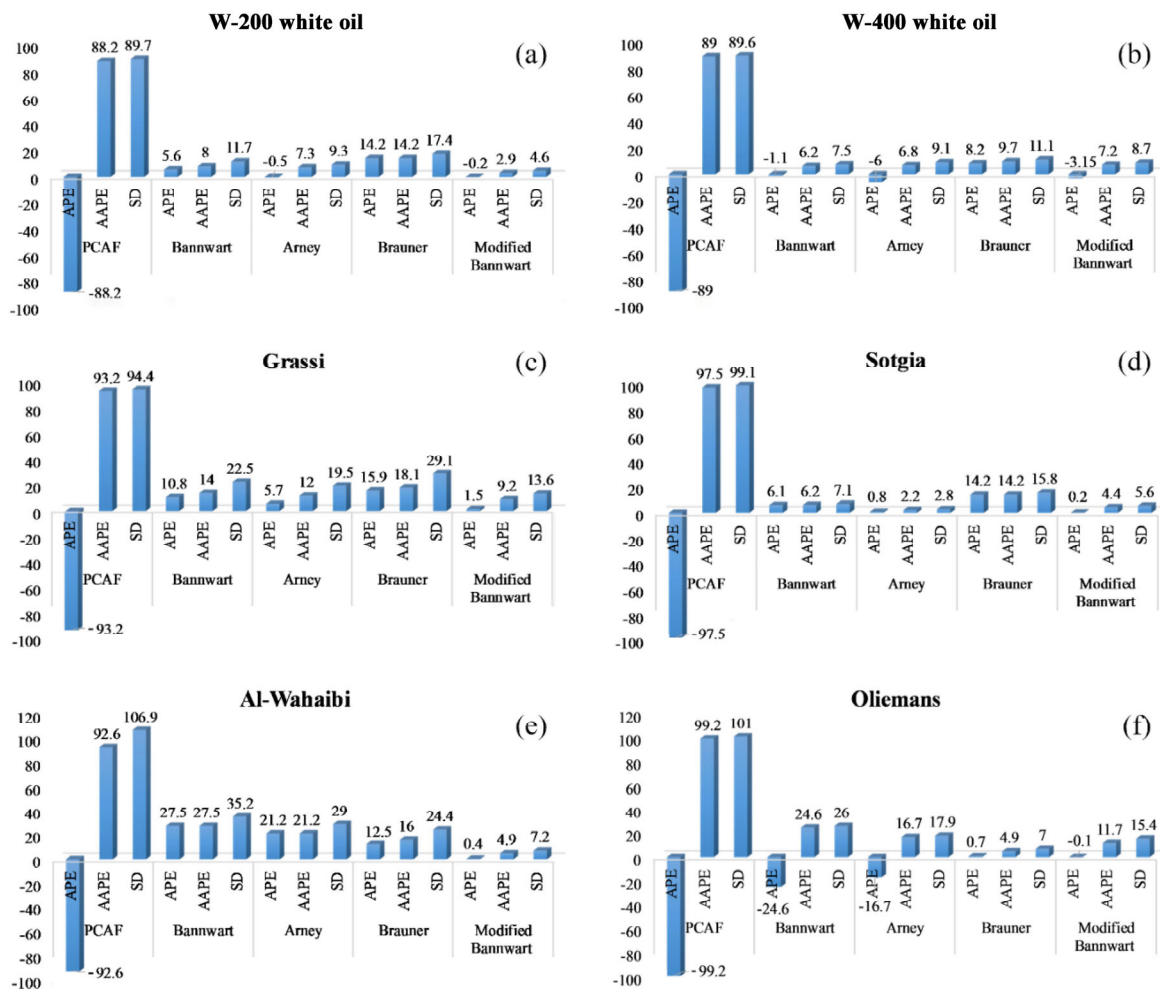


Fig. 6 Comparison of the accuracies of pressure gradient prediction of five models against experimental data from different sources: (a) W-200 white oil, (b) W-400 white oil, (c) Grassi et al. (2008), (d) Sotgia et al. (2008), (e) Al-Wahaibi et al. (2014), (f) Oliemans et al. (1985).

Table 3 Average APE, AAPE, SD for all experimental data

Model	Evaluation	Average of all experimental data (%)
PCAF model	APE	-93.3
	AAPE	93.3
	SD	96.8
Bannwart model	APE	4.1
	AAPE	14.4
	SD	18.3
Arney model	APE	0.8
	AAPE	11.0
	SD	14.6
Brauner model	APE	11.0
	AAPE	12.9
	SD	17.5
Modified Bannwart model	APE	-0.2
	AAPE	6.7
	SD	9.2

Oliemans. The new friction coefficient Eq. (25) has improved the prediction accuracy of the model, adding the effects of the oil fouling and eccentricity. As shown in Table 3, the average APE of the models for all sets of data decreased from 4.1% to -0.2% , the average AAPE from 14.4% to 6.7%, and the average SD from 18.3% to 9.2%.

The comparison between the pressure gradient predicted by the modified Bannwart model and experimental data is shown in Fig. 7. It is clear that the deviations of most of the data (87.4%) fall within $\pm 15\%$, which means the modified model is able to better predict the pressure gradient of CAF flow for different experimental conditions. The APE, AAPE, SD of the modified model are -1.46% , 6.29%, and 9.3%, respectively. In particular, the data with the smallest AAPE (2.9%) are from W-200 white oil. By contrast, the data with the largest AAPE (11.7%) are from Oliemans et al. It is probably because black oil is adopted in Oliemans et al.'s experiment while the others used white oil.

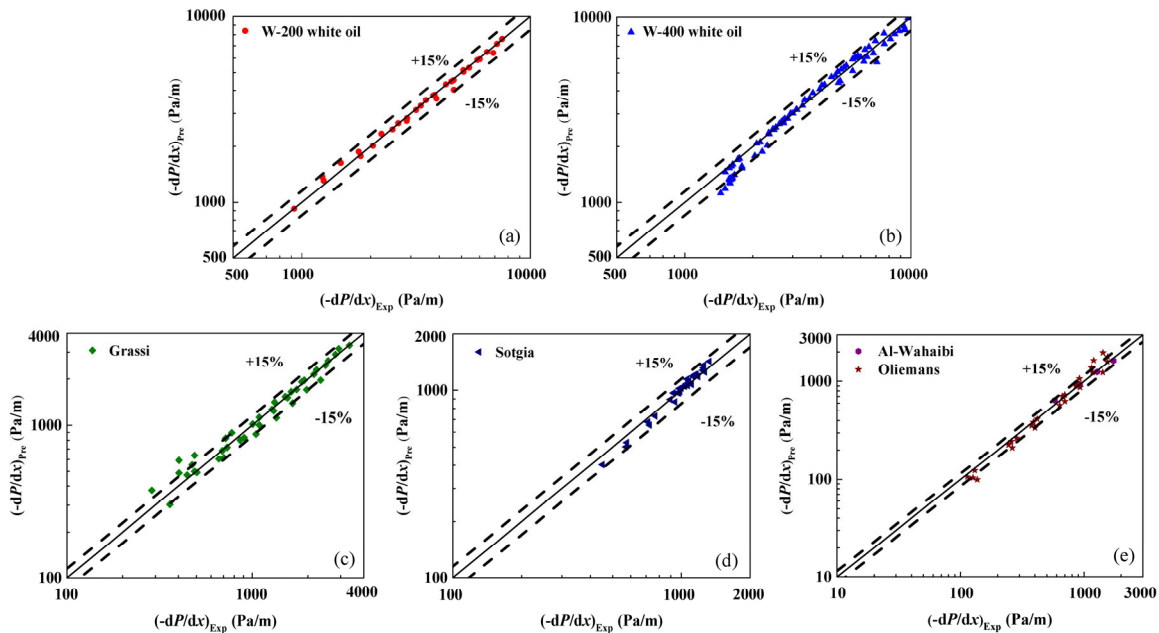


Fig. 7 Evaluation of the modified Bannwart model with 224 groups of data: (a) W-200 white oil, (b) W-400 white oil, (c) Grassi et al. (2008), (d) Sotgia et al. (2008), (e) Al-Wahaibi et al. (2014) and Oliemans et al. (1985).

4 Conclusions

Plexiglas pipes (14 mm) were adopted to study the flow patterns and pressure loss of oil–water flow using two types of white oil.

With the increase of the flow rate of water, the flow pattern transitioned from bubbly flow, plug flow, semi-annular flow to annular flow, and the oil core eccentricity was reduced. The flow pattern maps reveal that wave stratified flow (SW) only appears in the oil–water flow of W-200 white oil and the region of existence of Anw flow for W-400 white oil is larger than that for W-200 white oil.

A modified Bannwart model was put forward by improving the friction coefficient formula, which considered the effects of the oil fouling and eccentricity by proposing an empirical relationship combining the friction coefficient, Reynolds number, oil viscosity, and pipe wall roughness. When compared to the experimental results, it is found that the modified model is more precise than the original model and is the most precise one among the five models. By contrast, the prediction accuracy of the PCAF model is the lowest, for hypothesizing the water annulus as a laminar flow. The modified model is able to better predict the pressure gradient of CAF flow for different experimental conditions, for the deviations of 87.4% of data falling within $\pm 15\%$.

The data sources in this study are mainly focused on white oil, which makes the prediction accuracy of the modified model acceptable. The feasibility of the modified model into black oil should be further experimentally validated

in the future. Moreover, the adaptability of the model to the experiment condition of the steel pipe should also be investigated.

Acknowledgements

This work was supported by the National Natural Science Foundation of China (Grant Nos. 51779212 and 51911530129), Sichuan Science and Technology Program (Grant No. 2019YJ0350), China Postdoctoral Science Foundation funded project (Grant No. 2019M653483), and State Key Laboratory of Heavy Oil Processing (Grant No. SKLOP201901002).

References

- Al-Wahaibi, T. 2012. Pressure gradient correlation for oil–water separated flow in horizontal pipes. *Exp Therm Fluid Sci*, 42: 196–203.
- Al-Wahaibi, T., Al-Wahaibi, Y., Al-Ajmi, A., Al-Hajri, R., Yusuf, N., Olawale, A. S., Mohammed, I. A. 2014. Experimental investigation on flow patterns and pressure gradient through two pipe diameters in horizontal oil–water flows. *J Petrol Sci Eng*, 122: 266–273.
- Angeli, P., Hewitt, G. F. 1999. Pressure gradient in horizontal liquid–liquid flows. *Int J Multiphase Flow*, 24: 1183–1203.
- Arney, M. S., Bai, R., Guevara, E., Joseph, D. D., Liu, K. 1993. Friction factor and holdup studies for lubricated pipelining—I. Experiments and correlations. *Int J Multiphase Flow*, 19: 1061–1076.
- Bai, R. Y., Chen, K. P., Joseph, D. D. 1992. Lubricated pipelining: Stability of core–annular flow. Part 5. Experiments and comparison with theory. *J Fluid Mech*, 240: 97–132.
- Bannwart, A. C. 1999. A simple model for pressure drop in horizontal core annular flow. *J Braz Soc Mech Sci*, 21: 233–244.

- Bannwart, A. C. 2001. Modeling aspects of oil–water core–annular flows. *J Petrol Sci Eng*, 32: 127–143.
- Bannwart, A. C., Rodriguez, O. M. H., de Carvalho, C. H. M., Wang, I. S., Vara, R. M. O. 2004. Flow patterns in heavy crude oil–water flow. *J Energ Resour Technol*, 126: 184–189.
- Bensakhria, A., Peysson, Y., Antonini, G. 2004. Experimental study of the pipeline lubrication for heavy oil transport. *Oil Gas Sci Technol*, 59: 523–533.
- Brauner, N. 1991. Two-phase liquid–liquid annular flow. *Int J Multiphase Flow*, 17: 59–76.
- Brauner, N. 1998. 2.3.5 Multiphase fluid flow and pressure drop: Liquid–liquid two-phase flow. *Heat Exchanger Design Updates*, 5.
- Brauner, N., Moalem Maron, D. 1992. Stability analysis of stratified liquid–liquid flow. *Int J Multiphase Flow*, 18: 103–121.
- Brauner, N., Moalem Maron, D. 1999. Classification of liquid–liquid two-phase flow systems and the prediction of flow pattern maps. In: Proceedings of the 2nd International Symposium on Two-Phase Flow Modeling and Experimentation, 9: 747–754.
- Charles, M. E., Govier, G. W., Hodgson, G. W. 1961. The horizontal pipeline flow of equal density oil–water mixtures. *Can J Chem Eng*, 39: 27–36.
- Chen, N. H. 1979. An explicit equation for friction factor in pipe. *Ind Eng Chem Fundamen*, 18: 296–297.
- Georgiou, E., Maldarelli, C., Papageorgiou, D. T., Rumschitzki, D. S. 1992. An asymptotic theory for the linear stability of a core–annular flow in the thin annular limit. *J Fluid Mech*, 243: 653–677.
- Ghosh, S., Mandal, T. K., Das, G., Das, P. K. 2009. Review of oil water core annular flow. *Renew Sust Energ Rev*, 13: 1957–1965.
- Grassi, B., Strazza, D., Poesio, P. 2008. Experimental validation of theoretical models in two-phase high-viscosity ratio liquid–liquid flows in horizontal and slightly inclined pipes. *Int J Multiphase Flow*, 34: 950–965.
- Isaac, J. D., Speed, J. B. 1904. Method of piping fluids. U.S. Patent 759,374.
- Jain, A. K. 1976. Accurate explicit equation for friction factor. *J Hydr Eng Div*, 102: 674–677.
- Joseph, D. D., Bai, R. Y., Mata, C., Sury, K., Grant, C. H. R. I. S. 1999. Self-lubricated transport of bitumen froth. *J Fluid Mech*, 386: 127–148.
- Joseph, D. D., Renardy, M., Renardy, Y. 1984. Instability of the flow of two immiscible liquids with different viscosities in a pipe. *J Fluid Mech*, 141: 309–317.
- Lanier, D. 1998. Heavy oil: A major energy source for the 21st century. In: Proceedings of the 7th UNITAR International Conference on Heavy Crude and Tar Sands, 1: 361.
- Li, H. W., Wong, T. N., Skote, M., Duan, F. 2013. A simple model for predicting the pressure drop and film thickness of non-Newtonian annular flows in horizontal pipes. *Chem Eng Sci*, 102: 121–128.
- Marinescu, I. D., Rowe, W. B., Dimitrov, B., Ohmori, H. 2012. *Tribology of Abrasive Machining Processes*. William Andrew.
- Martínez-Palou, R., de Lourdes Mosqueira, M., Zapata-Rendón, B., Mar-Juárez, E., Bernal-Huicochea, C., de la Cruz Clavel-López, J., Aburto, J. 2011. Transportation of heavy and extra-heavy crude oil by pipeline: A review. *J Petrol Sci Eng*, 75: 274–282.
- McKibben, M. J., Gillies, R. G., Shook, C. A. 2000. Predicting pressure gradients in heavy oil–water pipelines. *Can J Chem Eng*, 78: 752–756.
- Moody, L. F. 1947. An approximate formula for pipe friction factors. *Trans ASME*, 69: 1005–1011.
- Oliemans, R. V. A., Ooms, G., Wu, H. L., Duijvestijn, A. 1987. Core–annular oil/water flow: The turbulent-lubricating-film model and measurements in a 5 cm pipe loop. *Int J Multiphase Flow*, 13: 23–31.
- Oliemans, R., Ooms, G., Wu, H., Duijvestijn, A. 1985. Core–annular oil/water flow: The turbulent-lubricating-film model and measurements in a 2-in pipe loop. In: Proceedings of the Middle East Oil Technical Conference and Exhibition, SPE-13725-MS.
- Ooms, G., Segal, A., van der Wees, A. J., Meerhoff, R., Oliemans, R. V. A. 1983. A theoretical model for core–annular flow of a very viscous oil core and a water annulus through a horizontal pipe. *Int J Multiphase Flow*, 10: 41–60.
- Prada, J. W. V., Bannwart, A. C. 2001. Modeling of vertical core-annular flows and application to heavy oil production. *J Energ Resour Technol*, 123: 194–199.
- Rodriguez, O. M. H., Bannwart, A. C. 2008. Stability analysis of core-annular flow and neutral stability wave number. *AIChE J*, 54: 20–31.
- Rodriguez, O. M. H., Bannwart, A. C., de Carvalho, C. H. M. 2009. Pressure loss in core–annular flow: Modeling, experimental investigation and full-scale experiments. *J Petrol Sci Eng*, 65: 67–75.
- Russell, T. W. F., Charles, M. E. 1959. The effect of the less viscous liquid in the laminar flow of two immiscible liquids. *Can J Chem Eng*, 37: 18–24.
- Saniere, A., Hénaut, I., Argillier, J. F. 2004. Pipeline transportation of heavy oils, a strategic, economic and technological challenge. *Oil Gas Sci Technol*, 59: 455–466.
- Schorle, B. J., Churchill, S. W., Shacham, M. 1980. Comments on: “An explicit equation for friction factor in pipe”. *Ind Eng Chem Fundamen*, 19: 228.
- Serghides, T. 1984. Estimate friction factor accurately. *Chem Eng*, 91: 63–64.
- Shi, J. 2015. A study on high-viscosity oil–water two-phase flow in horizontal pipes. Ph.D. Thesis. Cranfield University.
- Shi, J., Yeung, H. 2017. Characterization of liquid–liquid flows in horizontal pipes. *AIChE J*, 63: 1132–1143.
- Singh, V., Lo, S. 2010. Predicting pressure drop in pneumatic conveying using the discrete element modelling approach. *Prog Comput Fluid Dy*, 10: 334.
- Sotgia, G., Tartarini, P., Stalio, E. 2008. Experimental analysis of flow regimes and pressure drop reduction in oil–water mixtures. *Int J Multiphase Flow*, 34: 1161–1174.
- Strazza, D., Grassi, B., Demori, M., Ferrari, V., Poesio, P. 2011. Core–annular flow in horizontal and slightly inclined pipes: Existence, pressure drops, and hold-up. *Chem Eng Sci*, 66: 2853–2863.
- Tan, J. T., Jing, J. Q., Hu, H. L., You, X. Y. 2018. Experimental study of the factors affecting the flow pattern transition in horizontal oil–water flow. *Exp Therm Fluid Sci*, 98: 534–545.
- Tripathi, S., Bhattacharya, A., Singh, R., Tabor, R. F. 2015. Lubricated transport of highly viscous non-Newtonian fluid as core-annular flow: A CFD study. *Procedia IUTAM*, 15: 278–285.
- Zigrang, D. J., Sylvester, N. D. 1982. Explicit approximations to the solution of Colebrook’s friction factor equation. *AIChE J*, 28: 514–515.